A MULTI-SCALE, IMAGE-BASED PORE NETWORK MODELING APPROACH TO SIMULATE TWO-PHASE FLOW IN HETEROGENEOUS ROCKS

Tom Bultreys[1], Wesley De Boever[1], Luc Van Hoorebeke[2] and Veerle Cnudde[1]
[1]UGCT/PProGRess, Dept. of Geology and Soil Science, Ghent University, Krijgslaan 281 (S8), 9000, Ghent, Belgium
[2]UGCT/Radiation Physics, Dept. of physics and astronomy, Ghent University, Proeftuinstraat 86, 9000 Ghent, Belgium

This paper was prepared for presentation at the International Symposium of the Society of Core Analysts held in St. John's Newfoundland and Labrador, Canada, 16-21 August, 2015

ABSTRACT

Despite the large interest in the multi-phase flow properties of rocks with broad pore size distributions, most digital rock physics approaches struggle with the presence of multiple pore scales. In this work, we present a method to estimate relative permeability (K_r) and resistivity index (RI) curves of such heterogeneous rocks during drainage. In our dual pore network model (DPNM), macropores are represented as pores and throats , while unresolved microporosity is treated as a continuous porous medium. The scales are coupled by including microporosity as symbolic network elements in the DPNM, based on 3D image analysis. The validity of the method is investigated by treating two carbonate rocks (Estaillades and Savonnières limestone). We present a sensitivity analysis of the drainage behaviour of these networks on the microporosity's petrophysical properties, which are provided as input. While a number of challenges persist, the presented examples show how DPNM can help increase the understanding of two-phase flow in complex carbonate rocks.

INTRODUCTION

Pore scale modeling is becoming an important tool to study how multi-phase transport properties of core samples depend on the rock's microstructure and on the rock-fluid system (e.g. wettability). Thanks to the recent developments in imaging techniques like micro-computed tomography (micro-CT) [1], the pore space of many rock types can be imaged in 3D. In pore network modeling, a simplified network of pores and throats is extracted from these images. For low capillary numbers, two-phase flow can then be simulated on the pore network model (PNM) by applying quasi-static invasion percolation. The loss in detail caused by the simplification of pore space geometry and fluid mechanics is compensated by the method's high computational efficiency. Despite the large interest in image-based pore scale modeling, modeling multi-phase flow in heterogeneous materials (e.g. many carbonates and clay-bearing sandstones) with broad pore sizes remains problematic. The difficulties are mostly related to the sample size/resolution trade-off in both imaging and modeling. PNM are the most likely candidate for this type of modeling, due to their high computational efficiency and their

infinite resolution. In some dual pore network modeling (DPNM) approaches, individual pores from the different scales are coupled into one multi-scale network [2,3]. This approach offers a detailed description of the microporosity present, but quickly becomes computationally infeasible when pore sizes span several orders of magnitude. In contrast, the sub-resolution porosity can be treated as a continuous porous medium, characterized by upscaled properties (e.g. [4]). In the method presented here, we use the continuum approach for the microporosity to generate image-based multi-scale networks which allow simulations even when the macroporosity does not percolate.

MATERIALS AND METHODS

We present simulations performed on two monomineralic, calcitic French limestones. Estaillades limestone has a porosity of about 25 %, which contains intergranular macropores and intra-granular micropores in fossil grains [5]. Savonnières limestone is a layered oolithic limestone belonging to the Oolithe Vacuolaire, a stratigraphical unit which also includes Brauvilliers stone (among other varieties) [6]. Its pore structure contains 4 types of porosity: inter-granular and intra-oolithic microporosity, and inter-granular and micro-connected macroporosity (hollow ooliths) [7]. The hollow ooliths are only connected to the other macro-pores by microporosity in the oolith-shells. Depending on local variations, the permeability ranges from 115 mD to more than 2000 mD (based on TinyPerm mini-permeameter measurements), and porosity ranges from 22% to 41%.

Imaging

The pore space of an Estaillades sample of 7 mm and a Savonnières sample of 6 mm diameter were imaged with UGCT's HECTOR micro-CT scanner (developed in collaboration with XRE, Belgium) [8]. The former sample was scanned at an accelerating high voltage of 100 kV and a target power of 10W. 2800 projections (2s illumination each) were reconstructed with Octopus Reconstruction software (Inside Matters, Belgium). The scan had a voxel size of 3.1 µm. A 1000x1000x1001 section of the scan was treated with a binormal noise filter and segmented into 3 phases (pore, solid and microporous voxels) with a hysteresis thresholding algorithm in Octopus Analysis. The Savonnières sample was scanned at an accelerating voltage of 120 kV and a target power of 10W. 2400 projections (illumination time 1s) were acquired, resulting in a scan with 3.8 µm voxel size. A 1000x1000x1000 subsection was segmented with a gradient watershed thresholding algorithm in Avizo (FEI, France), after performing an anisotropic diffusion filter.

DPNM Extraction

To extract a DPNM, a single-scale PNM was first extracted from the macroporous voxels with a maximal ball algorithm [9]. Then, microporous voxels in the micro-CT image were clustered into connected regions. Any two nodes in the macropore network which touch the same microporous cluster were connected by adding a special network element, henceforth called "micro-link". The multi-scale PNM thus consist out of three types of network elements: macroporous nodes, macroporous links and micro-links.

For each micro-link, the contact surface area of the microporous region with the connected macropores is calculated by applying a marching cubes (MC) algorithm on the 3D three-phase image. Micro-link lengths are defined as the corresponding pore-to-pore distances. Figure 1 illustrates the imaging and network extraction workflow. Note that due to the applied network extraction method, microporous connections both parallel and in series to macroporous links are automatically taken into account. This is important, as serial microporous conductivity (dominant in rocks with pore-filling microporosity due to e.g. clay) was found to have different effects on the transport properties than parallel microporous conductivity (dominant in rocks with grain-filling microporosity due to e.g. partial grain dissolution) [10].

DPNM Simulations

To calculate capillary pressure (P_c) curves, K_r-curves and RI-curves on multi-scale networks, we modified the quasi-static network simulator developed at Imperial College [11]. This model performs an invasion-percolation algorithm to simulate the pore filling sequence during drainage, while neglecting the influence of viscous forces. At several points during this invasion simulation, the flowrates of both fluid phases are calculated separately by imposing a pressure difference over the network and assuming mass conservation of the fluids in each pore. This leads to a set of linear equations which can be solved for the pressure:

$$q_{ij} = g_{ij} \frac{P_i - P_j}{L_{ij}}$$
$$\sum_j q_{ij} = 0, \forall i \quad (1)$$

With q_{ij} the flow from pore i to pore j, g_{ij} the electrical or hydraulic conductance between pores i and j, L_{ij} the distance from pore i to pore j and P_j the pressure in pore j. Network elements have square, triangular or circular cross-sections and retain wetting films in the corners, which is important to correctly model the wetting phase connectivity.

The multi-scale PNM simulation extends this framework by taking into account micro-links. Flow through the microporosity is taken into account by assigning upscaled transport properties to these network elements. Therefore, the multi-scale simulations take a number of variable parameters of the microporosity as input rather than calculating them: porosity, P_c-curve, (relative) permeability, breakthrough capillary pressure (BCP) at a certain micro-link length, formation factor and saturation exponent. The advantage is that the model does not have to take each separate micropore into account, allowing to simulate larger volumes and thus incorporate more rock heterogeneity in the simulations. The transport properties of the coupled network are then calculated as described in the rest of this section (more details provided in [12]).

The saturation is calculated by summing the macroporous and the microporous saturation, the latter is extracted from the microporosity's P_c-curve. The porosity of the microporous phase is supplied as input, while the total volume of microporosity is

calculated on the micro-CT image. Macropores can be invaded with non-wetting fluid through a micro-link if a BCP is exceeded. This type of invasion is usually only important for macropores which are only connected to the inlet face of the network by taking into account microporous connectivity, as other macropores can be invaded through macro-throats (which have larger radii than the throats in the microporosity). If one would assume one single BCP for all micro-links, each macropore would be invaded instantaneously and simultaneously at a certain capillary pressure. To come to a more realistic drainage behavior, we try to mimic the behavior that a network with individual micropores would display. Each microlink is therefore regarded as a cuboid domain filled with a regular network of micropores. The hight of the cuboid is determined as the pore-to-pore distance, while the square base is set to match the average pore-microporous contact surface area of the micro-link. Scaling relations can then be deduced from percolation theory to find the breakthrough saturation at which the non-wetting phase percolates through this geometry, if a breakthrough saturation for a certain domain size is provided as input. This input value can be calculated from a representative single-scale network for the microporosity, informed by e.g. SEM imaging. The percolation threshold saturation is translated to a BCP for each micro-link by using the input capillary pressure curve for the microporosity. It should be noted that the approach followed here does not take correlated heterogeneity in the microporous network into account.

Permeabilities and electrical resistivities of the multi-scale network are calculated in the classical way (equation 1, [11]), but micro-links are also assigned a conductivity. Since the microporosity is treated as a continuous porous medium with known upscaled properties (which are provided as input), these conductivities can be calculated if a geometric shape is assigned to each micro-link. Micro-links are treated as truncated cones: the surface areas of the bases are set equal to the pore-micropore contact surface areas, and the length of the cone is set equal to the pore-to-pore distance. The electrical or hydraulic conductivity of the micro-link can then be calculated by taking into account this geometry, in combination with the microporosity's effective electrical conductance or effective permeability at its current wetting phase saturation:

$$g_{ij} = \frac{\sqrt{A_i \cdot A_j}}{\rho_{micro}(S_w) \cdot L_{ij}} \tag{2}$$

With A_i the contact surface area of the microporosity cluster to pore i, L_{ij} the distance from pore i to pore j, and $\rho_{micro}(S_w)$ the hydraulic or electric resistance of the microporosity at the current wetting saturation:

$$\rho_{hydr,p}(S_w) = \frac{\mu_p}{k \cdot k_{r,p}(S_w)} \tag{3}$$

$$\rho_{elec}(S_w) = R_w \cdot FF_{micro} \cdot S_w^{-n} \tag{4}$$

In these equations, μ_p and $k_{r,p}(S_w)$ are the viscosity and the relative permeability of fluid phase p (wetting or non-wetting), k is the absolute permeability, R_w is the resistivity of the wetting fluid, FF_{micro} the formation factor, and n the saturation exponent.For computational reasons, a maximum length for micro-links has to be set. All micro-links larger than this length are removed. This cut-off length also influences the results, as the simplifications made in the network model cause an overestimation of the microporous conductivity in long micro-links. Therefore, the cut-off length is chosen as the shortest length for which all micro-connected macropores can be drained appropriately. Eliminating this user-defined parameter is the subject of further research.

RESULTS AND DISCUSSION

For Estaillades, the microporosity's input P_c-curve was deduced from a mercury intrusion porosimetry (MIP) experiment. For Savonnières, this P_c-curve was based on the pore size distribution in [7]. For both cases, the input K_r-curve and BCP were assessed by simulations on an artificial network with a pore throat size distribution representative for the microporosity in each rock. The other microporosity input properties (Table 2) were based on [4] and [7], respectively.

Estaillades Limestone

In the Estaillades model, all macro-pores and throats were scaled with a factor 1.25 to correct for an overestimation of intrusion capillary pressure (likely due to segmentation uncertainty). Single-phase transport results calculated on the DPNM can be found in Table 1. K_r and RI results are compared to experimental measurements from [13,14] in Figure 2. DPNM simulations match the experimental trends better than single-scale PNM, showing the importance of including microporosity in the simulations. Differences between the experimental measurement and our results can be explained by sample scale, heterogeneity, and by the difficulty of assessing the input parameters. In this sample, the microporosity conducts mainly in parallel to the macroporosity. The model presented here and the model in [4] mainly differ in their treatment of serial microporous conductivity. As can be expected then, the RI results are in good agreement with the results presented in [4] and show double-bending behavior [14]. The K_r-results agree with the observations in [16] that added microporous pathways increase $K_{r,nw}$ and decrease $K_{r,w}$, and that this effect is stronger for higher microporous conductivities (see further).

Savonnières Limestone

In the investigated sample, the macropores in the hollow ooliths make up 30% of the macropore space. As these pores are only connected through microporosity, they are not taken into account when calculating transport properties with conventional, single-scale PNM. The P_c-curve simulated with the DPNM therefore matches the experimental P_c-curve (scaled from an MIP experiment on a different Savonnières sample) better than the single-scale PNM (Figure 3). The hollow ooliths start to drain at $S_w = 0.61$, when nearly all inter-granular macropores have been filled with non-wetting phase. The Kr-curve (Figure 3) is in qualitative agreement with measurements on Brauvilliers limestone [15],

which has a similar lithology than Savonnières but is tighter. The saturations at the cross-over K_r and at the onset of non-wetting phase flow are matched better with the DPNM than with the PNM, mostly due to the inclusion of the wetting saturation in microporosity. In the multi-scale network, the inter-granular macropores dominate the $K_{r,nw}$ behavior ($K_{r,nw}$ = 0.83 at S_w = 0.61). At S_w < 0,61, $K_{r,nw}$ bends down due to the lower importance of the microporosity/hollow ooliths pore system for the conductivity. In the RI-simulation (Figure 3), the bending-up behavior at S_w=0.3 in the single-scale simulation contradicts the classification of Brauvilliers as a texture III rock characterized by a double bending RI [14]. In the DPNM simulation however, the curve weakly bends up until reaching the macropores' percolation threshold (S_w = 0.61), and bends down when the pressure is further increased because the wetting films in the macropores become the dominant electrical pathways when the microporosity drains. The weakness of the bending-up may be an artifact of the selection of the length cut-off parameter. The simulations on Savonnières illustrate how our DPNM can be used when microporosity provides both parallel and serial connectivity to macroporosity.

Sensitivity study of P_c and K_r on microporosity properties

In this section, the influence of the microporosity's permeability, breakthrough saturation and capillary pressure curve on the relative permeability behavior of the multi-scale networks is investigated. Varying these properties helps to better understand the influence of microporosity on petrophysical properties of complex rocks. Furthermore, it allows to probe the sensitivity of the model to the microporosity's input properties which are often difficult to assess.

Influence of the microporosity's permeability

The microporosity's permeability was varied over 4 orders of magnitude for the Estaillades and the Savonnières network (Figure 4), while keeping all other parameters constant. With increasing microporous permeability, the non-wetting phase relative permeability decreases and the wetting phase relative permeability increases. This is due to the increasing importance of fluid flow through microporosity, which is only invaded by the non-wetting phase at S_w < 0.5 for Estaillades and S_w < 0.6 for Savonnieres. The behavior fits well with the observation that non-wetting phase mobility is enhanced and wetting phase mobility decreased by the existence of high-permeability pathways [16], in this case caused by the macroporous network.

Influence of the microporosity's breakthrough saturation

To test the influence of the input breakthrough saturation (and equivalently BCP) on a network where a significant amount of micro-links conduct in series to macro-throats, this parameter (defined for a 100x100x100 µm geometry) was varied for simulations with the Savonnières network. Drainage results for the different breakthrough saturations (Figure 5) show identical P_c-curves and K_r-curves for S_w down to 0.6, as macro-pores cannot be invaded through micro-links as long as the capillary pressure is below the microporosity's intrusion capillary pressure. The well-connected macropores are thus drained first. Below S_w = 0.6, P_c and K_r curves show minor differences, related to the fact

that disconnected macro-porosity (mostly hollow ooliths) start to fill at different capillary pressures for different microporous breakthrough saturations. The results show that this parameter is of particularly minor importance to the K_r-calculations in this network, if the pore sizes of the microporosity and the macroporosity do no significant overlap.

Influence of the microporosity's input capillary pressure curve

To assert how the microporosity's pore size distribution affects the drainage behavior in a multi-scale carbonate, the input capillary pressure curve in the Savonnières simulation was varied while keeping the other input parameters constant. Results with input capillary pressure curves corresponding to a scaling of the microporous throat sizes with factors 0.1, 2, 3, 4 and 5 were compared. Size distributions for micro-and macroporosity are shown in Figure 6. When microporous throat sizes are scaled with a factor 3 or more, there is significant overlap with the throat sizes of the macroporous network. This is an interesting test case, as it indicates how the model responds to situations where there is no clear distinction between the peaks in a rock's multimodal pore size distribution, or when the resolution of the imaging method (in this case micro-CT) cannot be tuned to a value in between the peaks. Scaling factors larger than 5 were not tested, as microporosity with throat sizes larger than the macroporosity would be unphysical.

When microporosity is scaled with a factor 0.1, all well-connected macropores are filled before the microporosity is invaded. This is clearly reflected in the P_c-curve by a strong increase in the capillary pressure at $S_w = 0.6$. The new flow paths which are opened to non-wetting phase flow below this saturation are less efficient, as they are associated with drainage of macropores which only contribute to the flow through connections with low-permeability micro-links. In the $K_{r,nw}$-curve (Figure 7), this point in the drainage sequence is characterized by a sharp bend. The influence on $K_{r,w}$ is much smaller, as the wetting phase flow is already limited by passage through wetting films in the (fully drained) well-connected macro-pore network.

For scaling factors larger than 1, the rise in the $K_{r,nw}$-curve shifts to lower wetting saturations (Figure 7). This behavior can be analyzed by looking at the relative permeability behavior of the macro-pore network separately ("classical network" in Figure 3). Due to its heterogeneous nature, the relative permeability of the macro-network has a sharp increase at a (macroporous) wetting saturation of 0.5. At this point, 70% of the well-connected macro-pore space has been drained. The slight shift for the multi-scale simulation with scaling factor 2 (Figure 7) can then be explained by taking into account that the microporosity's invasion capillary pressure is reached at $S_w = 0.72$ for this simulation. Therefore, at a given total wetting saturation below 0.72, the wetting saturation of the well-connected macro-network is higher than in the multi-scale simulation with the original microporosity's throat sizes (due to drainage of microporosity and, at lower saturation, of isolated macropores). For larger scaling factors, the microporosity also starts to significantly affect the invasion sequence of the well-connected macropores, due to the increased overlap in microporous and macroporous throat sizes. For scaling factor 3, the strong increase in permeability (at total $S_w = 0.65$)

only happens when 82% of the well-connected macropore space has been drained (compare to 70% in the original multi-scale network). This means that the well-connected macroporosity is drained through macro-throats and micro-links concurrently, and suggests that pores are not strictly drained in order of decreasing size of their connected macro-throats. More validation work is needed to investigate the physical relevance of the model in such situations.

CONCLUSION

In this work, we show a method to perform DPNM simulations with upscaled microporosity properties based on micro-CT scans of heterogeneous rocks. The employed method takes microporous conductivity into account by the concept of microlinks, and allows pores to be drained through microporous connectivity in the drainage simulation. While the method cannot be considered truly predictive yet, the presented simulations on real carbonates illustrate how the model can help to understand the influence of microporosity on transport properties, by investigating the influence of microporosity properties. Major remaining challenges are the current need to include a user defined micro-link cut-off parameter and the difficulty of assessing the upscaled petrophysical parameters for the microporosity.

ACKNOWLEDGEMENTS

Prof. Dr. M. Blunt and Dr. A.Q. Raeini are thanked for helping with the maximal ball code and the microPoreFlow code. Dr. H. Derluyn and Dr. M.A. Boone are acknowledged for their help with the Savonnières sample and its micro-CT scan, and Dr. J. Dils and Prof. Dr. G. Deschutter for the MIP measurements on Estaillades. The agency for Promotion of Innovation by Science and Technology in Flanders (IWT) is acknowledged for T. Bultreys' PhD grant.

REFERENCES

1. Cnudde V., M.N. Boone, "High-resolution X-ray computed tomography in geosciences: A review of the current technology and applications", *Earth-Science Rev.* (2013) **123**, 1–17.
2. Jiang Z., M.I.J. van Dijke, K.S. Sorbie, G.D. Couples, "Representation of multiscale heterogeneity via multiscale pore networks", *Water Resources Res.* (2013) **49**, 5437–5449.
3. Prodanović M., A. Mehmani, A.P. Sheppard, "Imaged-based multiscale network modelling of microporosity in carbonates", *Geol. Soc. London, Spec. Publ.* (2014) **406**, SP406–9.
4. Bauer D., S. Youssef, M. Fleury, S. Bekri, E. Rosenberg, O. Vizika, "Improving the Estimations of Petrophysical Transport Behavior of Carbonate Rocks Using a Dual Pore Network Approach Combined with Computed Microtomography", *Transp. Porous Media*. (2012) **94**, 505–524.

5. Youssef S., M. Han, D. Bauer, E. Rosenberg, S. Bekri, M. Fleury, O. Vizika, "High resolution µ-CT combined to numerical models to assess electrical properties of bimodal carbonates", (2008) 37, in: Int. Symp. Soc. Core Anal., Society of Core Analysts, Abu Dhabi UAE.
6. Derluyn H., M. Griffa, D. Mannes, I. Jerjen, J. Dewanckele, P. Vontobel, A. Sheppard, D. Derome, V. Cnudde, E. Lehmann, J. Carmeliet, "Characterizing saline uptake and salt distributions in porous limestone with neutron radiography and X-ray micro-tomography", *J. Build. Phys.* (2013) **36**, 353–374.
7. Roels S., J. Elsene, J. Carmeliet, H. Hens, "Characterisation of pore structure by combining mercury porosimetry and micrography", *Mater. Struct.* (2001) **34**, 76–82.
8. Masschaele B., M. Dierick, D. Van Loo, M.N. Boone, L. Brabant, E. Pauwels, V. Cnudde, L. Van Hoorebeke, "HECTOR: A 240kV micro-CT setup optimized for research", *J. Phys. Conf. Ser.* (2013) **463**, 012012.
9. Dong H., M. Blunt, "Pore-network extraction from micro-computerized-tomography images", *Phys. Rev. E*. (2009) **80**, 036307.
10. A. Mehmani, M. Prodanović, "The effect of microporosity on transport properties in porous media", *Adv. Water Resources*. (2014) **63**, 104–119.
11. Valvatne P.H., M.J. Blunt, "Predictive pore-scale modeling of two-phase flow in mixed wet media", *Water Resources Res.* (2004) **40**, W07406.
12. Bultreys T., L. Van Hoorebeke, V. Cnudde, "Multi-scale, micro-computed tomography-based pore network models to simulate drainage in heterogeneous rocks", *Adv. Water Resources*. (2015) **78**, 36–49.
13. Ott H., C.H. Pentland, S. Oedai, "CO2–brine displacement in heterogeneous carbonates", *Int. J. Greenh. Gas Control*. (2015) **33**, 135–144.
14. Han M., M. Fleury, P. Levitz, "Effect of the pore structure on resistivity index curves", (2007) 34, in: Int. Symp. Soc. Core Anal., Society of Core Analysts, Calgary CA.
15. Moctezuma-Berthier P., O. Vizika, P. Adler, "Water-oil relative permeability in vugular porous media: experiments and simulations", (2002) 06, in: Int. Symp. Soc. Core Anal., Society of Core Analysts, Monterey USA.
16. Bekri S., C. Laroche, O. Vizika, "Pore-network models to calculate transport properties in homogeneous and heterogeneous porous media", *Computational Methods in Water Resources, Proceedings of the XIVth International Conference*, Elsevier, Delft, Holland, (2002) **2**, 1115, Hassanizadeh, Schotting, Gray and Pinder, Elsevier

TABLES AND FIGURES

Table 1. Single phase flow properties of the two carbonates calculated with single-scale PNM, with DPNM and measured experimentally (experimental values for Estaillades from [4]).

	Estaillades	Savonnières
K PNM (mD)	281	244
K DPNM (mD)	289	268
K Exp. (mD)	273	903 (but heterogeneous)
FF PNM	36.8	85.7
FF DPNM	19.3	13.5
FF Exp.	24	-

Table 2. Input parameters for the DPNM.

	Estaillades	Savonnières
φ_{micro}	0.36	0.35
K_{micro}(mD)	8	4.1
FF_{micro}	7.72	8.2
BCP	0.3 for $(300\mu m)^3$ network	0.3 for $(100\mu m)^3$ network
Cut-off length (µm)	67.5	160

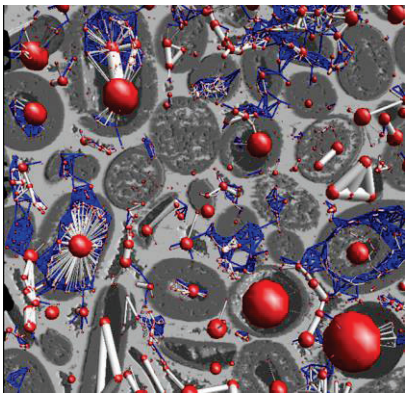

Figure 1. Illustration of DPNM extracted from avonnières limestone. Microporous zones are in dark grey, micro-links in blue.

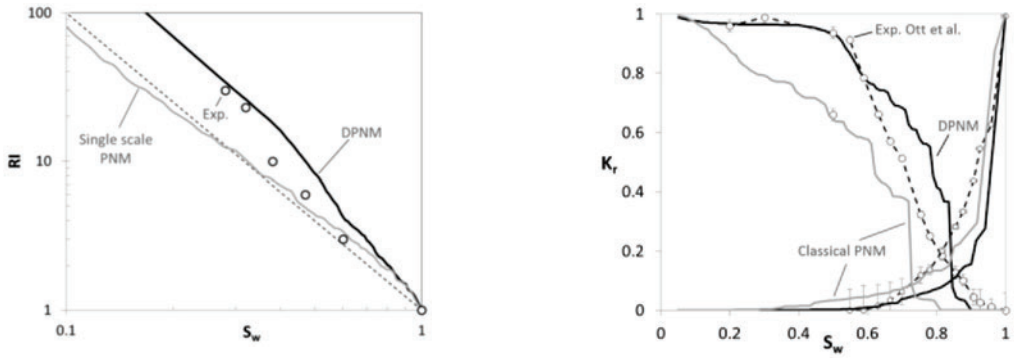

Figure 2. RI and Kr-curves for drainage of Estaillades calculated with a single scale maximal ball based PNM and with a DPNM, compared to experimental results from resp. [14] and [13] (the former estimated from the graph).

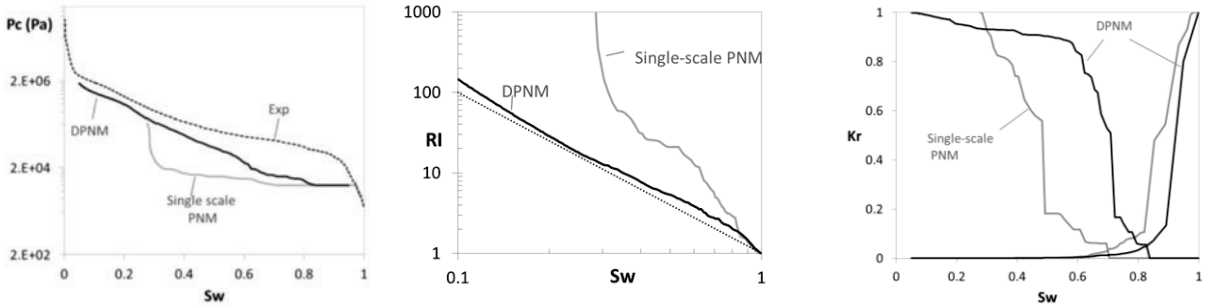

Figure 3. Pc-curve (left), RI-curve (middle) and K_r-curves (right) for drainage of Savonnières, calculated with a single scale maximal ball based PNM and with the proposed DPNM. The experimental Pc-curve is obtained from an MIP measurement.

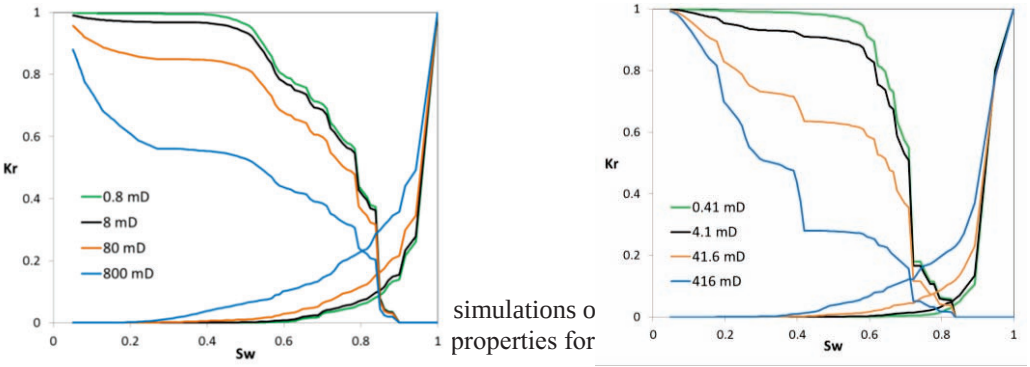

Figure 4. R simulations o the Savonni properties for

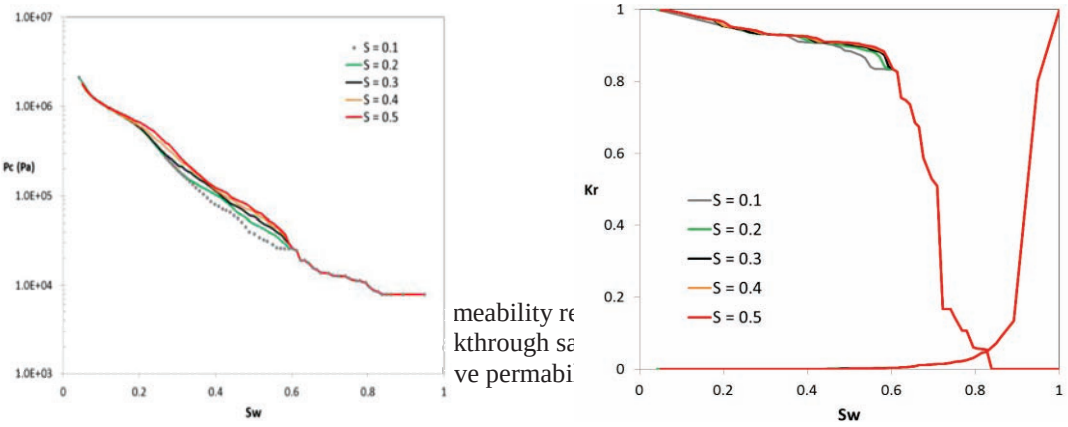

Figure 5. D meability re Savonnière kthrough sa geometry). ve permabi

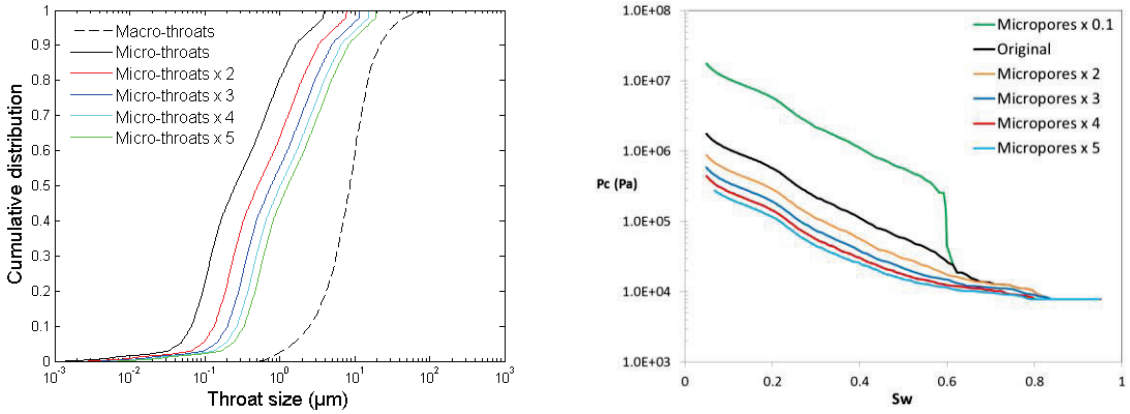

Figure 6. Cumulative pore size distributions and multi-scale drainage capillary pressure curves for different input microporosity Pc-curves in Savonnières.

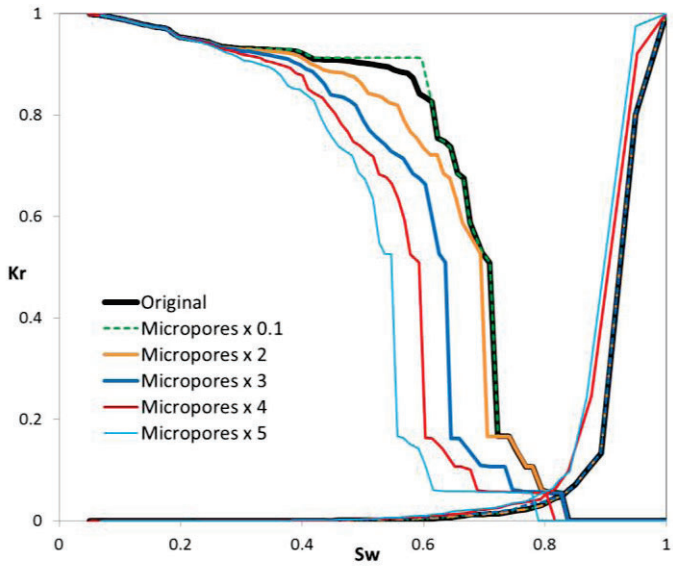

Figure 7. Drainage relative permeability curves calculated on the multi-scale Savonnières network with different microporosity P_c-curves as input. These input P_c-curves correspond to scaling of the throat sizes in the microporosity with different factors. The permeability of the microporosity was kept constant, to allow better interpretation of the results.